



# ODFNet: Using orientation distribution functions to characterize 3D point clouds

Yusuf H. Sahin<sup>a,\*\*</sup>, Alican Mertan<sup>a</sup>, Gozde Unal<sup>a</sup>

<sup>a</sup>*Istanbul Technical University, Computer Engineering, Istanbul, 34469, Turkey*

## ABSTRACT

Learning new representations of 3D point clouds is an active research area in 3D vision, as the order-invariant point cloud structure still presents challenges to the design of neural network architectures. Recent works explored learning either global or local features or both for point clouds, however none of the earlier methods focused on capturing contextual shape information by analysing local orientation distribution of points. In this paper, we leverage on point orientation distributions around a point in order to obtain an expressive local neighborhood representation for point clouds. We achieve this by dividing the spherical neighborhood of a given point into predefined cone volumes, and statistics inside each volume are used as point features. In this way, a local patch can be represented by not only the selected point's nearest neighbors, but also considering a point density distribution defined along multiple orientations around the point. We are then able to construct an orientation distribution function (ODF) neural network that involves an ODFBlock which relies on mlp (multi-layer perceptron) layers. The new ODFNet model achieves state-of-the-art accuracy for object classification on ModelNet40 and ScanObjectNN datasets, and segmentation on ShapeNet S3DIS datasets.

© 2020 Elsevier Ltd. All rights reserved.

## 1. Introduction

Convolutional neural networks (CNNs) are widely used in vision and pattern recognition problems like object classification, object recognition and segmentation (LeCun et al. (2015)). However, CNNs were not applicable to point clouds until recent years. The main obstacle behind this was how to interpret a point in a point cloud representation, which has a permutation-invariant structure, as opposed to pixels or voxels in 2D or 3D images. On a 2D or 3D image grid, the convolution operation is defined as a weighted sum in a local neighborhood, which is defined by the kernel. However, in a point cloud, a similar neighborhood structure among the points does not exist. PointNet (Qi et al. (2017a)) pioneered the way in utilizing neural network models for the point cloud classification problem by targeting a global feature transformation on all the points in the point cloud while respecting their order invariance. While PointNet did not use any neighborhood information, it is argued and shown that using local features improves the performance in recent works like Qi et al. (2017b); Deng et al. (2018); Xu et al. (2018).

Recently, in order to extract local features of point clouds, various approaches are presented such as creating spherical volumes (Qi et al. (2017b)) or choosing k-nearest neighbors (Wang et al. (2019)) and collecting local information of each point in those defined neighborhoods. The latest studies DensePoint (Liu et al. (2019b)) and ShellNet (Zhang et al. (2019)) that obtained state-of-the-art results for classification on the ModelNet40 classification benchmark (Wu et al. (2015)), create spherical regions around each point. DensePoint employs spheres of different sizes in each layer of the neural network to obtain features from multiple scales; whereas in ShellNet, coordinates of points in each shell are transformed via an mlp (multi-layer perceptron), and a max-pooling operation aggregates the features across shells. In both methods, the points in the sphere are handled regardless of their orientations with respect to the selected point. In Lei et al. (2019), a spherical convolution is presented alongside octree partitioning where the sphere is divided into bins, and features are obtained by averaging the features of the points inside the bin, without using any point density information.

In order to increase the representation capability of local features, we employ a point's neighboring orientation distribution that leads to a new representation named point Orientation Dis-

<sup>\*\*</sup>Corresponding author:  
e-mail: [sahinyu@itu.edu.tr](mailto:sahinyu@itu.edu.tr) (Yusuf H. Sahin)

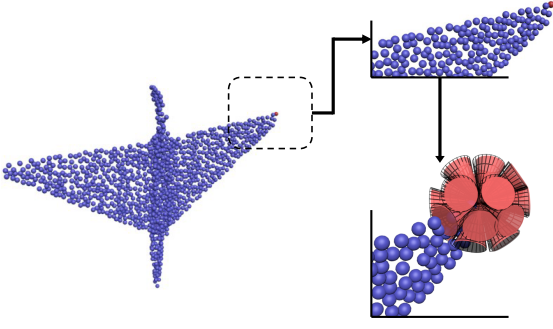


Fig. 1. A plane object from ModelNet40 (Wu et al. (2015)) dataset. For each point in a point cloud, ODFNet calculates the distribution of the neighbor points inside a spherical region. To do this, it benefits from cones with predefined orientations that span the spherical sectors. These cones can be of different scales and radii.

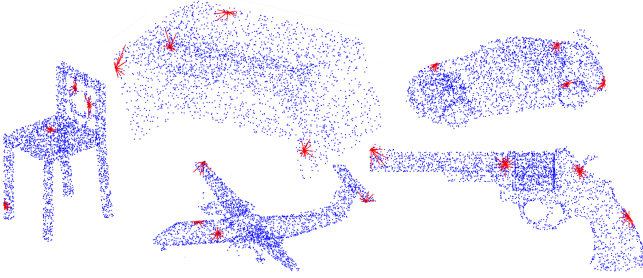


Fig. 2. ODFs for some selected points on example point clouds from ShapeNet (Yi et al. (2016)) dataset. Line length indicates strength.

tribution Functions (ODFs) for point clouds. ODFs can be computed by dividing each sphere around a point into a set of cones along predefined orientations, and calculating density of points in each cone, as depicted in Figure 1. To increase representability, overlapping cones are also included in calculations. Some example ODFs are given in Figure 2. It can be observed that the ODF at the tip of the gun object, the ODFs on the corners of the plane or the table, or on the surface of the car clearly capture and express the orientation density of points around the given point. Hence, in our design of a point cloud analysis network model, we utilize the ODFs with their enhanced capability to compactly summarize the local neighborhood structure of a point cloud to our advantage.

The main contributions of our work can be summarized as:

- Point ODFs which incorporate the directional information inside a spherical neighborhood is defined.
- A dedicated neural network architecture, the ODFNet, for classification and segmentation of point clouds is presented.
- ODFs for a point cloud provide a rotation invariant representation in the x-y plane.
- The ODFNet architecture is tested on popular benchmarks, and state-of-the-art (SoTA) accuracy on Model-

Net40, Shapenet(Yi et al. (2016)), S3DIS(Armeni et al. (2016)) and ScanObjectNN(Uy et al. (2019)) are obtained.

## 2. Related Works

Earlier studies like Sedaghat et al. (2016); Li et al. (2016); Maturana and Scherer (2015); Wu et al. (2015) focusing on classification of 3D objects prefer to voxelize the objects and use the voxelized occupancy map as an input to a neural network. However, this approach is not deemed efficient because of two reasons: First, the voxelization quality is highly related to selected grid spacing and as grid spacing dimensions get lower, distortion of a voxelized 3D object increases. Although high-resolution voxel grids are desired, they are impractical due to computational constraints. Considering the input as a 3D matrix, the network will consume significantly more storage and computation power when compared to 2D networks. A second drawback is that this is a very sparse representation, hence a superfluous amount of data is unnecessarily processed. Riegler et al. (2017) constructed a new representation to decrease the data amount by processing voxels, but the deformation problem remains.

Another approach is obtaining 2D images or depth maps and using them as inputs to a neural network (Sfikas et al. (2018); Su et al. (2015); Zanuttigh and Minto (2017); Guo et al. (2016)). However, this approach is not deemed favorable as well since complete object or scene information is not utilized.

In order to make use of the standard grid convolution operation from Euclidean CNN domain, Hua et al. (2018) projects a grid onto every point where filter kernels are placed, and features are calculated over those grids via the convolution operation. Li et al. (2018) presented an architecture that learns a transformation matrix which weighs and permutes the points to be used in grid convolution.

PointNet (Qi et al. (2017a)) is considered as the first attempt to use point clouds as raw inputs to a neural network. As it might be expected, the main difficulty of using directly the points instead of view renders or voxelized 3D maps comes from the set representation since all permutations on a point set describes the same entry. Hence in PointNet, to classify a point cloud, all points are processed in multi-layer perceptrons in parallel (i.e. as shared weights for all points) to obtain point features and a symmetric function (e.g. a max-pooling operation) is used over these features to obtain an aggregated global feature. Although studies like Hua et al. (2018) showed that ordered-points can be used without a symmetric function, the symmetric function notion is widely used (Deng et al. (2018); Yang et al. (2018)). Other studies using PointNet as a backbone network or in middle steps include (Zamorski et al. (2020); Deng et al. (2018)).

PointNet++ (Qi et al. (2017b)) focuses on the fact that the original PointNet loses local features since all points are treated independently until the max-pool step. Thus, they hierarchically sample and group the point cloud and implement mini PointNets for each group. Wang et al. (2019) introduce DGCNN that handles the point cloud as a graph and use a k-nearest neighbor approach to construct the connections. Then,

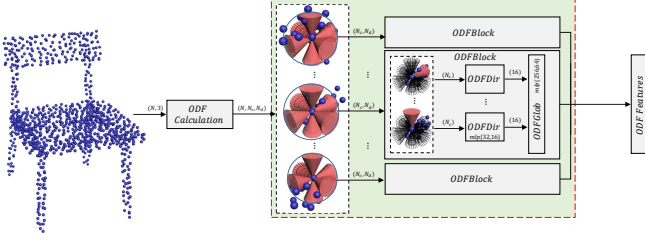


Fig. 3. The ODFBlock and its usage to obtain ODF features. Here  $N_c$  and  $N_d$  represent the number of different cones and directions, respectively. For every point, ODF values are computed along different cones. Then, ODF values are processed in ODFBlocks. An ODFBlock consists of two mlps: ODFDir and ODFGlob.

they define an edge convolution operation to perform a convolution centered on the selected point according to its nearest neighbors. In SpiderCNN (Xu et al. (2018)), a new convolution operation which benefits from Taylor series expansion is presented. In KPConv (Thomas et al. (2019)), kernel points with learnable weights are defined inside a local neighborhood and a linear correlation between a kernel point position and a neighbor point position is calculated and multiplied by these weights. In DensePoint (Liu et al. (2019b)) and ShellNet (Zhang et al. (2019)), also a dedicated convolution is defined relying on statistics inside local neighborhoods, particularly spherical regions. Lei et al. (2019) designed a procedure where spherical regions are divided into bins and point features for each bin are collected according to bin weights. Then mean of the point features of each bin is used as bin features. For further detailed reading on point clouds, Guo et al. (2019)’s survey can be investigated. In the point cloud processing literature, the lack of any orientation-specific local feature representation motivated us to propose the ODFNet in this work, which is explained in the next section.

### 3. Method: ODFBlock and ODFNet

Our approach relies upon Orientation Distribution Functions due to their capability to express directional properties of local point cloud structure. In this section, we first describe the ODFs, the dedicated ODFBlock which is depicted in Figure 3, and then we present the ODFNet.

Our inspiration of ODFs used in this work is mainly based on an analogy to diffusion orientation distribution functions calculated and commonly utilized in analysis of brain white matter tissue based on diffusion MRI (Tuch (2004)). Similarly, ODFs constructed through intensity flux measurements over oriented cylinders around a centerline point can facilitate vascular segmentation as in (Cetin and Unal (2015)). Whereas those works relied on image intensities for estimation of underlying fiber or vessel orientations, for a point cloud, we rely on the number of points in a local conic neighborhood at multiple orientations. Furthermore, to capture the local point density information in a hierarchy of scales, we utilize multi-scale cones with different apex angles and heights.

In order to make the proposed ODF representation more

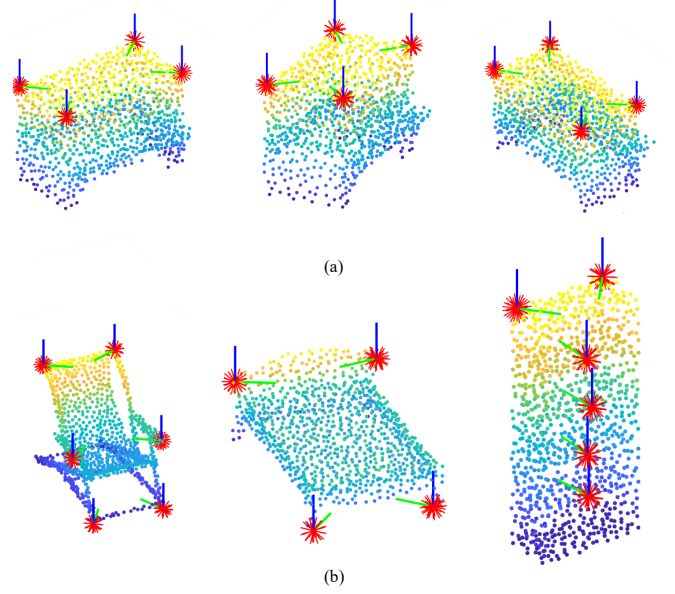


Fig. 4. ODF directions according to nearest neighbors are depicted. Green arrows indicate pivot and blue arrows indicate the z axis. (a) By rotating the objects in x-y plane, ODF values do not change since the directions are aligned with respect to rotation invariant pivots. (b) For symmetric points of the same object, nearly symmetric pivot directions are obtained.

adaptive to orientation changes of the objects, in calculation of the ODFs, pivot directions need to be selected. For every point, projection of the selected point’s 32 nearest neighbors on the x-y plane are calculated and the most dense direction is selected as the pivot. Using the pivot direction and the z-axis, the ODF directions are aligned. In Figure 4, some pivot directions are shown. In addition to this alignment’s contribution to obtain a rotation invariant representation for rotations in the x-y plane (Figure 4.a), it also leads to symmetric representations for symmetric points (Figure 4.b).

Specifically, in order to compute ODF values at a point  $x_i$  along each direction  $v_l$ , we utilize multiple cones as illustrated in Figure 5. For a specific cone with an apex angle  $2\alpha_k$ , height  $d_n$ , and cone’s center direction vector  $v_l$ , the ODF is calculated at  $x_i \in S$ , where  $S$  denotes the set of all points, as follows:

$$ODF(x_i, \alpha_k, d_n, v_l) = \sum_{x_j \in S, i \neq j} \mathbb{1}(\|x_i - x_j\|_2 < d_n) \cdot \mathbb{1}\left(\arccos\left(\frac{(x_i - x_j) \cdot v_l}{\|x_i - x_j\| \|v_l\|}\right) < \alpha_k\right) \quad (1)$$

which gives us the point count inside the selected cone. Here,  $\mathbb{1}(\cdot)$  refers to the indicator function. Since the cone heights  $d_n$  are selected according to  $n^{\text{th}}$ -neighbor distance, this value is then normalized by  $n$ . Parameter  $n$  is selected from a collection of  $[8, 16, 24, 32]^{\text{th}}$  neighbors.

For cone orientations  $v_l$ , 42 orientations that are obtained after first tessellation of an icosahedron are used as default. This is selected empirically by observing that further increasing the amount of tessellation causes a high rate of intersection between the cones and reducing it decreases the representation

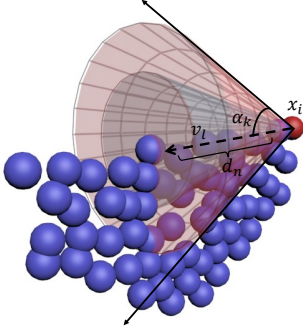


Fig. 5. An example ODF cone is placed on  $x_i$  along direction  $v_l$ . Cones at multiple scales (of heights and apex angles) are used to capture point density features at a hierarchy of neighborhoods.

power. For apex angles  $\alpha_k$ , the smallest angle that leads to covering of the whole sphere 31.71 and 60 degrees are used. Thus, for every cone orientation, in overall, 8 different cones are obtained (4 different distances  $d_n$  and 2 apex angles  $\alpha_k$ ). In our experiments on a single NVIDIA Titan RTX graphics card, calculation of the cone values takes under  $\sim 76$  msecs for a point cloud of 1024 points despite its complex information. It is also advantageous that the representation is calculated only once in the network.

In a point cloud, those differently sized and oriented cones that we construct help capture local variations in terms of point density, and encode them into the ODF features, which is provided into the dedicated neural network block in Figure 3. After calculating the ODFs at each point, we define the ODFBlock which operates on the ODFs as follows:

$$ODFBlock(x_i, \theta_d, \theta_g) = ODFGlob(\theta_d, ODFDir(\theta_g, ODF(x_i))) \quad (2)$$

where  $ODF(x_i)$  in short denotes a tensor of point density values  $ODF(x_i, \alpha_k, d_n, v_l)$  for different cones along a collection of direction vectors in  $\mathbb{S}^2$ . Parameters  $\theta_d = [\theta_d^1, \theta_d^2, \dots, \theta_d^m]$ , and  $\theta_g = [\theta_g^1, \theta_g^2, \dots, \theta_g^p]$  are learnable parameters of the ODFBlock.  $ODFDir$  is an mlp that embeds the ODF tensor through aggregating features by collecting features of each direction, and  $ODFGlob$  is another mlp which aggregates the output embedding over all directions to obtain the aggregate ODFBlock output features.

### 3.1. ODFNet Network Model

To exploit our point ODF’s representation capability over point clouds, we design different ODFNets, which benefit from ODFs as well as point locations to capture both local and global features of point clouds and, which can be used for classification and segmentation tasks. As depicted in Figure 6, ODFNet first calculates the ODFs for each point as given by Equation 1 for  $N_c$  cones rotated around  $N_d$  direction vectors. Then for each point it benefits from two different mlps inside ODFBlock: ODFDir and ODFGlob. For differently scaled cones placed along the same direction, ODFDir calculates features capturing the point density along that direction. ODFGlob then operates on the features captured by ODFDir in order to fuse those

features and the result is later concatenated with the point coordinates.

In the blocks shown as *ODFNeigs* in Figure 6, in a similar manner with DGCNNs (Wang et al. (2019)), each point’s features are combined with its nearest neighbors’ features and the distance features.

For the classification task, the last layers of the architecture includes a max-pooling operation to produce a global feature vector describing the shape. After three fully connected layers, class scores are obtained at the output. For part segmentation in ShapeNet, the ODFNet architecture makes use of the categorical vector, which indicates the one-hot-coded object class. It is fed to the segmentation part of the ODFNet, as in Wang et al. (2019) and Qi et al. (2017a). The output size of the final output layer in both tasks depends on the number of object classes and object parts. For semantic segmentation in S3DIS, nearly the same architecture with part classification is used. However, since the dataset also includes RGB color information, colors and color distances are also used to obtain distance features and location features.

## 4. Experimental Results

In this section, we present the details of the experiments and performance evaluation results for ODFNet on classification and segmentation tasks <sup>1</sup>. We select widely used benchmark datasets and evaluate the ODFNet model over those, in order to provide comparison with the existing methods. Particularly, we experiment and report results on ModelNet40 and ScanObjectNN for classification, ShapeNet for part segmentation, and S3DIS for scene segmentation.

### 4.1. Shape Classification

For shape classification, we evaluated our model on ModelNet40 (Wu et al. (2015)) which consists of mesh models for 40 different categories and ScanObjectNN (Uy et al. (2019)) which contains 3D real life scans for 13 different object categories which also contains noise and missing parts.

**ModelNet:** For each mesh model, 1024 points are used as presented in Qi et al. (2017a) and scaled to fit in a unit sphere. Recent works prefer to do scaling and translation (Liu et al. (2019b)), scaling and perturbing (Wang et al. (2019)) and only perturbing (Zhang et al. (2019)) for data augmentation during training. Instead, nonuniform scaling, flipping in x and y directions and rotation by multiples of 90 degrees are applied. Also before the last classification block, randomly 512 points are selected for each object before max pooling at train time. Since the classification features are obtained by a max pooling layer, the deletion operation does not affect the network structure. The ODFs are calculated regardless of this operation to avoid shape inconsistencies. To make a fair comparison with the previous work, we compared our study with the methods that use only 1024 points for each object. The results in Table 1 show that,

<sup>1</sup>The source code for our ODFNet model will be provided at the time of publication.



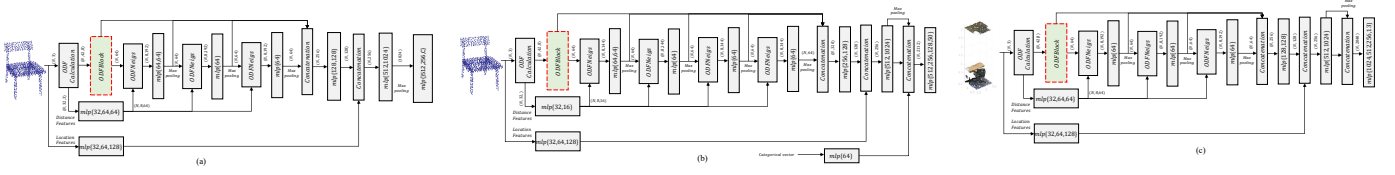


Fig. 6. ODFNet architecture used for (a) classification, (b) part segmentation and (c) scene segmentation. Letter *c* in first figure represents class count.

Table 1. Overall Accuracies (OA) for point cloud classification results on ModelNet40 dataset. (p: points, n: normals)

Method	input	OA
PointNet (Qi et al. (2017a))	p	89.2
PointNet++ (Qi et al. (2017b))	p+n	90.7
Kd-network (Klokov and Lempitsky (2017))	p	91.8
SpiderCNN (Xu et al. (2018))	p+n	92.4
Point2Seq (Liu et al. (2019a))	p	92.6
InterpCNN (Mao et al. (2019))	p	93.0
PointwiseCNN (Hua et al. (2018))	p	86.1
ShapeContextNet (Xie et al. (2018))	p	90.0
KCNet (Shen et al. (2018))	p	91.0
PointCNN (Li et al. (2018))	p	92.2
ShellNet (Zhang et al. (2019))	p	93.1
DGCNN (Wang et al. (2019))	p	92.9
DensePoint (Liu et al. (2019b))	p	93.2
ODFNet	p	<b>93.4</b>

Table 2. Classification accuracy scores for different tasks in ScanObjectNN (Uy et al. (2019)) dataset.

Model	OBJ_BG	PB_T25	PB_T25R	PB_T50R	PB_T50RS	OBJ_ONLY
3DmFV (Ben-Shabat et al. (2018))	68.2	67.1	67.4	63.5	63.0	73.8
PointNet (Qi et al. (2017a))	73.3	73.5	72.7	68.2	68.2	79.2
SpiderCNN (Xu et al. (2018))	77.1	78.1	77.7	73.8	73.7	79.5
PointNet++ (Qi et al. (2017b))	82.3	82.7	81.4	79.1	77.9	84.3
DGCNN (Wang et al. (2019))	82.8	83.3	81.5	80.0	78.1	86.2
PointCNN (Li et al. (2018))	86.1	83.6	82.5	78.5	78.5	85.5
ODFNet	<b>90.0</b>	<b>88.9</b>	<b>86.7</b>	<b>84.1</b>	<b>85.1</b>	<b>89.6</b>

our implementation outperforms other methods by an overall accuracy score of 93.4% via a single prediction.

**ScanObjectNN:** To evaluate the ODFNet on ScanObjectNN, an augmentation procedure similar to the ModelNet experiments is used. However, because the object point counts are larger here, 1024 points are randomly selected at train time. There are five different tasks: OBJ\_ONLY, OBJ\_BG, PB\_T25, PB\_T25R, PB\_T50R and PB\_T50RS. In OBJ\_BG, objects with background noise are classified. OBJ\_ONLY consists of objects having no background noise. The other sets are augmented versions of OBJ\_BG. Comparing our results with the scores given in Uy et al. (2019), the ODFNet model produces SoTA accuracy scores as can be observed in Table 2.

**Further Experiments:** To further investigate our network’s capacity for point cloud object abstraction, for each test subject, we extract the output of the last classification layer for the ODFNet, as well as for DensePoint and ShellNet, where the latter two are the previous SoTA point cloud architectures. Then, using two widely utilized dimensionality reduction techniques, UMAP (McInnes et al. (2018)) and t-SNE (Maaten and Hinton (2008)), we project those vectors onto 2D space and assess this

Table 3. Silhouette scores for last layers of ODFNet, DGCNN and ShellNet after UMAP McInnes et al. (2018) and t-SNE Maaten and Hinton (2008) projection. {worst:best}:{-1:1}

Method	tSNE S. Score	UMAP S. Score
ODFNet	<b>0.623</b>	<b>0.660</b>
DensePoint	0.453	0.474
ShellNet	0.472	0.466

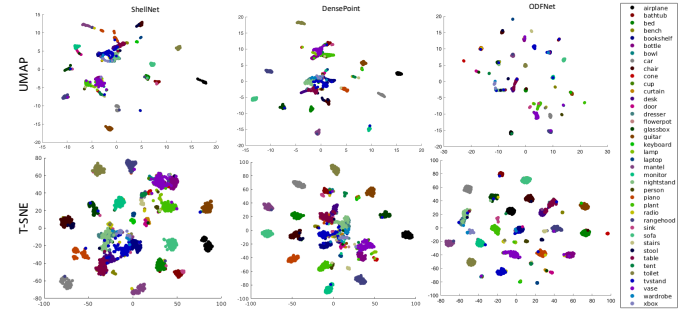


Fig. 7. The projections from the last layer outputs of ODFNet, DensePoint and ShellNet architectures for ModelNet40 dataset onto a 2D space using the UMAP McInnes et al. (2018) and t-SNE Maaten and Hinton (2008) methods.

mapping by the Silhouette score (Rousseeuw (1987)), which evaluates whether each object is well matched to its own cluster. The scores are given in Table 3, and the projections are visualized in Figure 7. As can be seen from the results, although quantitative scores on classification of these methods are close to each other, ODFNet’s features appear more distinctive and produce a relatively more separated layout than the other two methods, which is also observed in the Silhouette scores.

Furthermore, to understand which points generate global features at the classification step, features before the last max pooling of the network are examined. Heat maps according to contribution of each point to the final result are obtained for ODFNet and DG-CNN as given in Figure 8. It can be observed that the ODFNet selects a more diverse and seemingly important feature points from the point clouds when compared to the DG-CNN.<sup>2</sup> According to the visual results, we can conclude that for objects with relatively more complex geometric shapes, visually representative points, which are mostly corner and end

<sup>2</sup>Pointwise heat maps cannot be created for DensePoint and ShellNet since they do not use directly the points but their distribution.

Method	input	mpIoU	mIoU	a.plane	bag	cap	car	chair	e.phone	guitar	knife	lamp	laptop	m.bike	mug	pistol	rocket	s.board	table
Qi et al. (2017a)	p	80.4	83.7	83.4	78.7	82.5	74.9	89.6	73.0	91.5	85.9	80.8	95.3	65.2	93.0	81.2	57.9	72.8	80.6
Qi et al. (2017b)	p+n	81.9	85.1	82.4	79.0	87.7	77.3	90.8	71.8	91.0	85.9	83.7	95.3	71.6	94.1	81.3	58.7	76.4	82.6
Wang et al. (2019)	p	<b>84.6</b>	85.2	84.0	83.4	86.7	77.8	90.6	74.7	91.2	87.5	82.8	95.7	66.3	94.9	81.1	63.5	74.5	82.6
Atzmon et al. (2018)	p	81.8	85.1	82.4	80.1	85.5	<b>79.5</b>	90.8	73.2	91.3	86.0	85.0	95.7	73.2	94.8	<b>83.3</b>	51.0	75.0	81.8
Liu et al. (2019b)	p	84.2	86.4	84.0	<b>85.4</b>	<b>90.0</b>	79.2	91.1	<b>81.6</b>	91.5	87.5	84.7	95.9	74.3	94.6	82.9	<b>64.6</b>	76.8	<b>83.7</b>
Liu et al. (2019a)	p	82.2	85.2	82.6	81.8	87.5	77.3	90.8	77.1	91.1	86.9	83.9	95.7	70.8	94.6	79.3	58.1	75.2	82.8
ODFNet	p	83.3	<b>86.5</b>	<b>85.1</b>	85.0	89.5	78.7	<b>91.9</b>	73.6	<b>92.2</b>	<b>88.2</b>	<b>85.9</b>	<b>96.1</b>	<b>74.9</b>	<b>95.3</b>	82.2	53.7	<b>77.7</b>	83.3

Table 4. ShapeNet Part segmentation results for different architectures. Input column indicates whether points (p) and normals (n) are used.

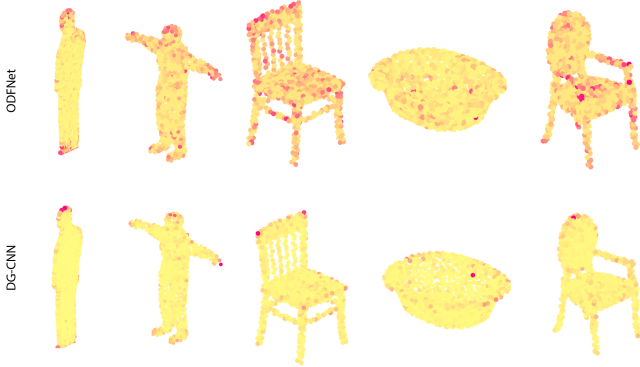


Fig. 8. Different heat maps for DG-CNN and ODFNet.

points, are selected by the ODFNet. The ODFs for those points that are around corners and edges have anisotropic distributions while the ODFs on the flat areas have isotropic distributions with similar strengths over many directions.

#### 4.2. Part Segmentation

We evaluated our segmentation network on ShapeNet part segmentation benchmark Yi et al. (2016), which contains 14007 training and 1874 test samples, 16 object categories each of them partitioned into  $\{2 - 6\}$  parts, making a total of 50 parts. Following the practice of the previous SoTA (Liu et al. (2019b)), which used ensembling, during testing phase, for every test object, we also obtain scaled versions of test objects by  $+0.3\%$ ,  $-0.3\%$  in each direction and averaged their scores. We compare our performance with those studies using a point cloud structure. Our experimental results for ShapeNet part segmentation are reported for ODFNet along with previous methods in Table 4.

#### 4.3. Scene Segmentation

For scene segmentation, the commonly used S3DIS dataset (Armeni et al. (2016)) is utilized. The dataset contains point clouds sampled from six different challenging scenes. General practice in experimentation with this dataset involves training with a leave-one-out cross validation (6-fold) strategy. SoTA results are obtained for S3DIS as shown in Table 5.

## 5. Discussions and Conclusion

Our experimental results demonstrate that ODFNet achieves the SoTA performance in both the classification task and particularly for the more challenging segmentation task in ShapeNet

Table 5. Overall accuracies and mIoU values for point cloud scene segmentation results on S3DIS dataset.

Method	mIoU	OA
PointNet (Qi et al. (2017a))	78.6	47.6
PointNet++ (Qi et al. (2017b))	81.0	54.5
PointSIFT (Jiang et al. (2018))	88.7	70.2
Engelmann (Engelmann et al. (2018))	84.0	58.3
3DContextNet (Zeng and Gevers (2018))	84.9	55.6
PointWeb (Zhao et al. (2019))	87.3	66.7
ShellNet (Zhang et al. (2019))	87.1	66.8
PointCNN (Li et al. (2018))	88.1	65.4
InterpCNN (Mao et al. (2019))	88.7	66.7
DGCNN (Wang et al. (2019))	84.1	56.1
(Liu et al. (2020))	88.5	64.1
RandLA-Net (Hu et al. (2020))	88.0	70.0
HEPIN (Jiang et al. (2019))	88.2	67.8
PointWeb (Zhao et al. (2019))	87.3	66.7
CF-SIS (Wen et al. (2020))	88.0	74.0
ODFNet	<b>90.8</b>	<b>72.2</b>

and S3DIS. This provides evidence to our hypothesis that the ODF representation, which exploits the idea of incorporation of local point orientation distribution characteristics into the point cloud neural network models, is highly beneficial.

The point orientation distribution features help the neural network models capture further informative characteristics of the point cloud. This is revealed by the attention that the ODFNet model pays to the unique identifying points on an object such as corners, tips, and borders between planar regions. Features generated by the ODFNet correlate with an increased representation power for point clouds.

The ODF representation for point clouds introduces a desired rotation-invariance property. We note that this is achieved only in the x-y plane, which adequately addresses the requirements of 3D scanning sensor positioning that stays roughly on the ground plane or on land vehicles.

As for future work, in geometric representation learning of point clouds, capturing essential defining characteristics of an object, whether through better augmented definitions of local patches around points as the ODFNet does, or in other similarly effective ways of local and global encoding schemes, could provide further improvements in supervised and unsupervised learning tasks on point clouds.

## References

Armeni, I., Sener, O., Zamir, A.R., Jiang, H., Brilakis, I., Fischer, M., Savarese, S., 2016. 3d semantic parsing of large-scale indoor spaces, in: Proceedings

- of the IEEE Conference on Computer Vision and Pattern Recognition, pp. 1534–1543.
- Atzmon, M., Maron, H., Lipman, Y., 2018. Point convolutional neural networks by extension operators. *arXiv preprint arXiv:1803.10091*.
- Ben-Shabat, Y., Lindenbaum, M., Fischer, A., 2018. 3dmfv: Three-dimensional point cloud classification in real-time using convolutional neural networks. *IEEE Robotics and Automation Letters* 3, 3145–3152.
- Cetin, S., Unal, G., 2015. A higher-order tensor vessel tractography for segmentation of vascular structures. *IEEE transactions on medical imaging* 34, 2172–2185.
- Deng, H., Birdal, T., Ilic, S., 2018. Ppfnet: Global context aware local features for robust 3d point matching, in: *Proceedings of the IEEE Conference on Computer Vision and Pattern Recognition*, pp. 195–205.
- Engelmann, F., Kontogianni, T., Schult, J., Leibe, B., 2018. Know what your neighbors do: 3d semantic segmentation of point clouds, in: *Proceedings of the European Conference on Computer Vision (ECCV)*, pp. 0–0.
- Guo, H., Wang, J., Gao, Y., Li, J., Lu, H., 2016. Multi-view 3d object retrieval with deep embedding network. *IEEE Transactions on Image Processing* 25, 5526–5537.
- Guo, Y., Wang, H., Hu, Q., Liu, H., Liu, L., Bennamoun, M., 2019. Deep learning for 3d point clouds: A survey. *arXiv preprint arXiv:1912.12033*.
- Hu, Q., Yang, B., Xie, L., Rosa, S., Guo, Y., Wang, Z., Trigoni, N., Markham, A., 2020. Randla-net: Efficient semantic segmentation of large-scale point clouds, in: *Proceedings of the IEEE/CVF Conference on Computer Vision and Pattern Recognition*, pp. 11108–11117.
- Hua, B.S., Tran, M.K., Yeung, S.K., 2018. Pointwise convolutional neural networks, in: *Proceedings of the IEEE Conference on Computer Vision and Pattern Recognition*, pp. 984–993.
- Jiang, L., Zhao, H., Liu, S., Shen, X., Fu, C.W., Jia, J., 2019. Hierarchical point-edge interaction network for point cloud semantic segmentation, in: *Proceedings of the IEEE International Conference on Computer Vision*, pp. 10433–10441.
- Jiang, M., Wu, Y., Zhao, T., Zhao, Z., Lu, C., 2018. Pointsift: A sift-like network module for 3d point cloud semantic segmentation. *arXiv preprint arXiv:1807.00652*.
- Klokov, R., Lempitsky, V., 2017. Escape from cells: Deep kd-networks for the recognition of 3d point cloud models, in: *Proceedings of the IEEE International Conference on Computer Vision*, pp. 863–872.
- LeCun, Y., Bengio, Y., Hinton, G., 2015. Deep learning. *nature* 521, 436–444.
- Lei, H., Akhtar, N., Mian, A., 2019. Octree guided cnn with spherical kernels for 3d point clouds, in: *Proceedings of the IEEE Conference on Computer Vision and Pattern Recognition*, pp. 9631–9640.
- Li, Y., Bu, R., Sun, M., Wu, W., Di, X., Chen, B., 2018. Pointcnn: Convolution on x-transformed points, in: *Advances in Neural Information Processing Systems*, pp. 820–830.
- Li, Y., Pirk, S., Su, H., Qi, C.R., Guibas, L.J., 2016. Fpnn: Field probing neural networks for 3d data, in: *Advances in Neural Information Processing Systems*, pp. 307–315.
- Liu, J., Yu, M., Ni, B., Chen, Y., 2020. Self-prediction for joint instance and semantic segmentation of point clouds, in: *European Conference on Computer Vision*, Springer. pp. 187–204.
- Liu, X., Han, Z., Liu, Y.S., Zwicker, M., 2019a. Point2sequence: Learning the shape representation of 3d point clouds with an attention-based sequence to sequence network, in: *Proceedings of the AAAI Conference on Artificial Intelligence*, pp. 8778–8785.
- Liu, Y., Fan, B., Meng, G., Lu, J., Xiang, S., Pan, C., 2019b. Densepoint: Learning densely contextual representation for efficient point cloud processing, in: *Proceedings of the IEEE International Conference on Computer Vision*, pp. 5239–5248.
- Maaten, L.v.d., Hinton, G., 2008. Visualizing data using t-sne. *Journal of machine learning research* 9, 2579–2605.
- Mao, J., Wang, X., Li, H., 2019. Interpolated convolutional networks for 3d point cloud understanding, in: *Proceedings of the IEEE International Conference on Computer Vision*, pp. 1578–1587.
- Maturana, D., Scherer, S., 2015. Voxnet: A 3d convolutional neural network for real-time object recognition, in: *Intelligent Robots and Systems (IROS)*, 2015 IEEE/RSJ International Conference on, IEEE. pp. 922–928.
- McInnes, L., Healy, J., Melville, J., 2018. Umap: Uniform manifold approximation and projection for dimension reduction. *arXiv preprint arXiv:1802.03426*.
- Qi, C.R., Su, H., Mo, K., Guibas, L.J., 2017a. Pointnet: Deep learning on point sets for 3d classification and segmentation, in: *Proceedings of the IEEE Conference on Computer Vision and Pattern Recognition*, pp. 652–660.
- Qi, C.R., Yi, L., Su, H., Guibas, L.J., 2017b. Pointnet++: Deep hierarchical feature learning on point sets in a metric space, in: *Advances in neural information processing systems*, pp. 5099–5108.
- Riegler, G., Ulusoy, A.O., Geiger, A., 2017. Octnet: Learning deep 3d representations at high resolutions, in: *Proceedings of the IEEE Conference on Computer Vision and Pattern Recognition*, pp. 3577–3586.
- Rousseeuw, P.J., 1987. Silhouettes: a graphical aid to the interpretation and validation of cluster analysis. *Journal of computational and applied mathematics* 20, 53–65.
- Sedaghat, N., Zolfaghari, M., Amiri, E., Brox, T., 2016. Orientation-boosted voxel nets for 3d object recognition. *arXiv preprint arXiv:1604.03351*.
- Sfikas, K., Pratikakis, I., Theoharis, T., 2018. Ensemble of panorama-based convolutional neural networks for 3d model classification and retrieval. *Computers & Graphics* 71, 208–218.
- Shen, Y., Feng, C., Yang, Y., Tian, D., 2018. Mining point cloud local structures by kernel correlation and graph pooling, in: *Proceedings of the IEEE conference on computer vision and pattern recognition*, pp. 4548–4557.
- Su, H., Maji, S., Kalogerakis, E., Learned-Miller, E., 2015. Multi-view convolutional neural networks for 3d shape recognition, in: *Proceedings of the IEEE international conference on computer vision*, pp. 945–953.
- Thomas, H., Qi, C.R., Deschaud, J.E., Marcotegui, B., Goulette, F., Guibas, L.J., 2019. Kpconv: Flexible and deformable convolution for point clouds. *arXiv preprint arXiv:1904.08889*.
- Tuch, D.S., 2004. Q-ball imaging. *Magnetic Resonance in Medicine: An Official Journal of the International Society for Magnetic Resonance in Medicine* 52, 1358–1372.
- Uy, M.A., Pham, Q.H., Hua, B.S., Nguyen, T., Yeung, S.K., 2019. Revisiting point cloud classification: A new benchmark dataset and classification model on real-world data, in: *Proceedings of the IEEE International Conference on Computer Vision*, pp. 1588–1597.
- Wang, Y., Sun, Y., Liu, Z., Sarma, S.E., Bronstein, M.M., Solomon, J.M., 2019. Dynamic graph cnn for learning on point clouds. *ACM Transactions on Graphics (TOG)* 38, 146.
- Wen, X., Han, Z., Youk, G., Liu, Y.S., 2020. Cf-sis: Semantic-instance segmentation of 3d point clouds by context fusion with self-attention, in: *Proceedings of the 28th ACM International Conference on Multimedia*, pp. 1661–1669.
- Wu, Z., Song, S., Khosla, A., Yu, F., Zhang, L., Tang, X., Xiao, J., 2015. 3d shapenets: A deep representation for volumetric shapes, in: *Proceedings of the IEEE conference on computer vision and pattern recognition*, pp. 1912–1920.
- Xie, S., Liu, S., Chen, Z., Tu, Z., 2018. Attentional shapecontextnet for point cloud recognition, in: *Proceedings of the IEEE Conference on Computer Vision and Pattern Recognition*, pp. 4606–4615.
- Xu, Y., Fan, T., Xu, M., Zeng, L., Qiao, Y., 2018. Spidernn: Deep learning on point sets with parameterized convolutional filters, in: *Proceedings of the European Conference on Computer Vision (ECCV)*, pp. 87–102.
- Yang, Y., Feng, C., Shen, Y., Tian, D., 2018. Foldingnet: Point cloud auto-encoder via deep grid deformation, in: *Proceedings of the IEEE Conference on Computer Vision and Pattern Recognition*, pp. 206–215.
- Yi, L., Kim, V.G., Ceylan, D., Shen, I., Yan, M., Su, H., Lu, C., Huang, Q., Sheffer, A., Guibas, L., et al., 2016. A scalable active framework for region annotation in 3d shape collections. *ACM Transactions on Graphics (TOG)* 35, 210.
- Zamorski, M., Zieba, M., Klukowski, P., Nowak, R., Kurach, K., Stokowiec, W., Trzcinski, T., 2020. Adversarial autoencoders for compact representations of 3d point clouds. *Computer Vision and Image Understanding* 193, 102921.
- Zanuttigh, P., Minto, L., 2017. Deep learning for 3d shape classification from multiple depth maps, in: *Proceedings of IEEE International Conference on Image Processing (ICIP)*.
- Zeng, W., Gevers, T., 2018. 3dcontextnet: Kd tree guided hierarchical learning of point clouds using local and global contextual cues, in: *Proceedings of the European Conference on Computer Vision (ECCV)*, pp. 0–0.
- Zhang, Z., Hua, B.S., Yeung, S.K., 2019. Shellnet: Efficient point cloud convolutional neural networks using concentric shells statistics, in: *Proceedings of the IEEE International Conference on Computer Vision*, pp. 1607–1616.
- Zhao, H., Jiang, L., Fu, C.W., Jia, J., 2019. Pointweb: Enhancing local neighborhood features for point cloud processing, in: *Proceedings of the IEEE Conference on Computer Vision and Pattern Recognition*, pp. 5565–5573.